Cross-scale interactions between electron and ion temperature gradient driven turbulence via sub-ion-scale structures

S. Maeyama[1], T.-H. Watanabe[1], Y. Idomura[2], M. Nakata[3], A. Ishizawa[4], M. Nunami[3]

[1] Nagoya University, Nagoya, Aichi, 464-8601, Japan
[2] Japan Atomic Energy Agency, Kashiwa, Chiba, 277-0871, Japan
[3] National Institute for Fusion Science, Toki, Gifu, 509-5292, Japan
[4] Kyoto University, Uji, Kyoto, 611-0011, Japan

E-mail: smaeyama@p.phys.nagoya-u.ac.jp

March 2016

Abstract. Multi-scale plasma turbulence including electron and ion temperature gradient modes (ETG/ITG) has been investigated by means of electromagnetic gyrokinetic simulations. Triad transfer analyzes on nonlinear mode coupling reveal cross-scale interactions between electron and ion scales. One of the interactions is suppression of electron-scale turbulence by ion-scale turbulence, where ITG-driven short-wave-length eddies act like shear flows and suppress ETG turbulence. Another cross-scale interaction is enhancement of ion-scale turbulence in presence of electron-scale turbulence. This is caused via short-wave-length zonal flows which are created by passing kinetic electron response in ITG, suppress ITG by their shearing, and are damped by ETG turbulence. In both cases, sub-ion-scale structures between electron and ion scales play important roles in the cross-scale interactions.

PACS numbers: 52.65.Tt, 52.30.Gz, 52.35.Ra

Keywords: gyrokinetics, Vlasov simulation, nonlinear interaction, multi-scale

Submitted to: *Nucl. Fusion*

1. Introduction

Plasma turbulence inherently involves multi-scale physics covering electron and ion scales characterized by their gyroradii. Since their scales are different by a factor of $\sim \sqrt{m_\mathrm{i}/m_\mathrm{e}}$ when their temperatures are the same, the most of previous literature assumed separation of their scales and analyzed single-scale turbulence driven by electron or ion temperature gradient modes (ETG or ITG). Recent simulation studies, however, resolve multi-scale ETG/ITG turbulence and suggest existence of the cross-scale interactions.

Although several mechanisms have already been discussed, e.g., mutually exclusive competition between ITG and ETG [1], stabilization of ITG by ETG-driven zonal flow [2], stabilization of ETG by short-wave-length ITG eddies and its weak back reaction to ITG [3], the understanding on the physical mechanisms of cross-scale interaction is still insufficient. The gyrokinetic simulation is a powerful tool to investigate the multi-scale ETG/ITG plasma turbulence. The early work by Jenko in 2004 employed Tokamak edge-like parameters and showed the coexistence of ITG and ETG [4]. In 2007, Candy and Waltz carried out simulations with employing Tokamak core parameters and found the suppression of ETG by ITG [5, 6]. Short while later, Görler reported ETG transport can survive when the linear growth rate of ITG is relatively small [7]. Although the above simulations employed reduced ion-to-electron mass ratio $m_\mathrm{i}/m_\mathrm{e} = 400$ or 900, recent progress of supercomputer technology and parallel computation algorithm allows us to access the realistic mass ratio $m_\mathrm{i}/m_\mathrm{e} = 1836$ for proton and 3670 for deuteron. The cross-scale interactions are observed even in these realistic mass ratio cases where the scales of electron and ion gyroradii separate further. A series of works by Howard et al. on the comparison between Alcator C-Mod experiments and multi-scale ETG/ITG simulations indicate that realistic mass ratio and cross-scale interactions between ETG and ITG can be essential for explaining experimental transport levels [8, 9]. Besides, multi-scale electromagnetic simulations by Maeyama et al. with the realistic mass ratio and β value confirm not only the suppression of ETG by ITG but also enhancement of ion-scale transport by electron-scale turbulence when ITG is stabilized by finite-β effects [10, 11]. The latest report from DIII-D experiments with ITER baseline parameters also suggests that cross-scale interactions must be accurately described to predict the performance of ITER burning plasma [12]. To promote the understanding on complex behaviors of cross-scale interactions, detailed analyses on nonlinear mode-to-mode coupling are indispensable.

In this context, this paper discuss in details the new aspect of physical mechanisms of cross-scale interactions in multi-scale ETG/ITG turbulence by Maeyama et al. The remainder of the paper is outlined as follows. In Sec. 2, we briefly describe our simulation model and develop diagnostic methods of nonlinear mode-to-mode transfer for the analysis of cross-scale interactions. In Sec. 3, simulation results demonstrate the existence of mutual cross-scale interactions. By means of the nonlinear transfer diagnostics, effects of ion-scale turbulence to electron-scale turbulence (the $i \to e$ interaction) is investigated in detail, and vice versa (the $e \to i$ interaction). In Sec. 4, the identified physical mechanisms of the cross-scale interactions are summarized. The cross-scale interactions are understood as successive nonlinear interactions between electron and ion scales via intermediate sub-ion-scale structures.

2. Methods

2.1. Governing equations

Micro-instabilities and turbulence associated with the anomalous transport in magnetic fusion plasma are well described by the electromagnetic gyrokinetics. The gyrokinetic Vlasov equation for the perturbed gyrocenter distribution function $\tilde{f}_\mathrm{s}(\boldsymbol{x}, v_\parallel, \mu, t) = \sum_{\boldsymbol{k}} \tilde{f}_{\mathrm{s}\boldsymbol{k}} e^{i\boldsymbol{k}\cdot\boldsymbol{x}}$ of the plasma species s [$= e$ (electron), i (ion)] is expanded

in the perpendicular wave number space,

$$\frac{\partial \tilde{f}_{\mathrm{s}\boldsymbol{k}}}{\partial t} + \left(v_\parallel \nabla_\parallel + i\boldsymbol{k}\cdot\boldsymbol{v}_{\mathrm{ds}} - \frac{\mu \nabla_\parallel B}{m_{\mathrm{s}}} \frac{\partial}{\partial v_\parallel} \right) \tilde{f}_{\mathrm{s}\boldsymbol{k}} + \mathcal{N}_{\mathrm{s}\boldsymbol{k}}$$
$$= -\frac{e_{\mathrm{s}} F_{\mathrm{Ms}}}{T_{\mathrm{s}}} \left[v_\parallel \left(\nabla_\parallel J_{0\mathrm{s}\boldsymbol{k}} \tilde{\phi}_{\boldsymbol{k}} + \frac{\partial J_{0\mathrm{s}\boldsymbol{k}} \tilde{A}_{\parallel \boldsymbol{k}}}{\partial t} \right) \right.$$
$$\left. + i\boldsymbol{k}\cdot\boldsymbol{v}_{\mathrm{ds}} J_{0\mathrm{s}\boldsymbol{k}} \tilde{\phi}_{\boldsymbol{k}} - i\boldsymbol{k}\cdot\boldsymbol{v}_{*\mathrm{s}} J_{0\mathrm{s}\boldsymbol{k}} (\tilde{\phi}_{\boldsymbol{k}} - v_\parallel \tilde{A}_{\parallel \boldsymbol{k}}) \right] + \mathcal{C}_{\mathrm{s}\boldsymbol{k}}, \tag{1}$$

where $\boldsymbol{v}_{\mathrm{ds}} = \boldsymbol{b} \times (\mu \nabla B + m_{\mathrm{s}} v_\parallel^2 \boldsymbol{b}\cdot\nabla \boldsymbol{b})/(e_{\mathrm{s}} B)$ and $\boldsymbol{v}_{*\mathrm{s}} = \boldsymbol{b} \times [T_{\mathrm{s}} \nabla \ln n_{\mathrm{s}} + (m_{\mathrm{s}} v_\parallel^2/2 + \mu B - 3T_{\mathrm{s}}/2) \nabla \ln T_{\mathrm{s}}]/(e_{\mathrm{s}} B)$ denote the magnetic and diamagnetic drift velocities. $\boldsymbol{E} \times \boldsymbol{B}$ and magnetic flutter nonlinearities are represented by $\mathcal{N}_{\mathrm{s}\boldsymbol{k}} = -\sum_{\boldsymbol{p}} \sum_{\boldsymbol{q}} \delta_{\boldsymbol{p}+\boldsymbol{q},\boldsymbol{k}} (\boldsymbol{b}\cdot \boldsymbol{p}\times\boldsymbol{q}/B) J_{0\mathrm{s}\boldsymbol{p}} (\tilde{\phi}_{\boldsymbol{p}} - v_\parallel \tilde{A}_{\parallel \boldsymbol{p}})(\tilde{f}_{\mathrm{s}\boldsymbol{q}} + e_{\mathrm{s}} F_{\mathrm{Ms}} J_{0\mathrm{s}\boldsymbol{q}} \tilde{\phi}_{\boldsymbol{q}}/T_{\mathrm{s}})$. A collision operator employed here is the gyrophase-averaged Lenard-Bernstein model collision operator $\mathcal{C}_{\mathrm{s}\boldsymbol{k}} = \nu_{\mathrm{s}} [\partial_{v_\parallel} (v_\parallel \tilde{f}_{\mathrm{s}\boldsymbol{k}} + v_{\mathrm{ts}}^2 \partial_{v_\parallel} \tilde{f}_{\mathrm{s}\boldsymbol{k}}) + (1/v_\perp) \partial_{v_\perp} (v_\perp^2 \tilde{f}_{\mathrm{s}\boldsymbol{k}} + v_{\mathrm{ts}}^2 v_\perp \partial_{v_\perp} \tilde{f}_{\mathrm{s}\boldsymbol{k}}) - k_\perp^2 \rho_{\mathrm{ts}}^2 \tilde{f}_{\mathrm{s}\boldsymbol{k}}]$ [13], whose velocity-space-derivative terms describe a drag force and diffusion in velocity space, conserve local particle density, and yields a Maxwell distribution as an equilibrium state, while the last term represents the classical diffusion with the coefficient $\nu_{\mathrm{s}} \rho_{\mathrm{ts}}^2$. The perturbed electrostatic and parallel vector potentials $\tilde{\phi}_{\boldsymbol{k}}, \tilde{A}_{\parallel \boldsymbol{k}}$ are determined by the gyrokinetic Poisson and Ampère equations

$$\left[k_\perp^2 + \frac{1}{\varepsilon_0} \sum_{\mathrm{s}} \frac{e_{\mathrm{s}}^2 n_{\mathrm{s}}}{T_{\mathrm{s}}} (1 - \Gamma_{0\mathrm{s}\boldsymbol{k}}) \right] \tilde{\phi}_{\boldsymbol{k}}$$
$$= \frac{1}{\varepsilon_0} \sum_{\mathrm{s}} e_{\mathrm{s}} \int dv^3 J_{0\mathrm{s}\boldsymbol{k}} \tilde{f}_{\mathrm{s}\boldsymbol{k}}, \tag{2}$$

$$k_\perp^2 \tilde{A}_{\parallel \boldsymbol{k}} = \mu_0 \sum_{\mathrm{s}} e_{\mathrm{s}} \int dv^3 J_{0\mathrm{s}\boldsymbol{k}} v_\parallel \tilde{f}_{\mathrm{s}\boldsymbol{k}}, \tag{3}$$

where the gyrophase-average operators are $J_{0\mathrm{s}\boldsymbol{k}} = J_0(k_\perp \rho_{\mathrm{s}})$ and $\Gamma_{0\mathrm{s}\boldsymbol{k}} = I_0(k_\perp^2 \rho_{\mathrm{ts}}^2) \exp(-k_\perp^2 \rho_{\mathrm{ts}}^2)$ with the gyroradius $\rho_{\mathrm{s}} = m_{\mathrm{s}} v_\perp/(e_{\mathrm{s}} B)$. We employ the local flux-tube model in a circular tokamak (or so-called $s-\alpha$) geometry with the flux coordinates $x = r - r_0$, $y = (r_0/q_0)[q\theta - \zeta]$, $z = \theta$ (where the minor radius r, poloidal and toroidal angles θ, ζ), while the parallel velocity $v_\parallel$ and the magnetic moment μ are used as velocity-space coordinates. Time evolution of the perturbed distribution function and electromagnetic fields are numerically solved by the gyrokinetic Vlasov simulation code GKV [14]. Recent extension of its computational capability enables multi-scale ETG/ITG turbulence simulations [15].

2.2. Entropy balance and gyrokinetic triad transfer

Multiplying $T_{\mathrm{s}} \tilde{f}_{\mathrm{s}\boldsymbol{k}}^*/F_{\mathrm{Ms}} + e_{\mathrm{s}} J_{0\mathrm{s}\boldsymbol{k}} \tilde{\phi}_{\boldsymbol{k}}^*$ to Eq. (1) and integrating it over the velocity space and along the field aligned coordinate, one derives the entropy balance relation [16] for each mode,

$$\frac{d}{dt} (S_{\boldsymbol{k}} + W_{\boldsymbol{k}}) = X_{\boldsymbol{k}} + D_{\boldsymbol{k}} + E_{\boldsymbol{k}} + I_{\boldsymbol{k}}. \tag{4}$$

From the left, the perturbed entropy $S_{\boldsymbol{k}}$, the perturbed field energy $W_{\boldsymbol{k}}$, the turbulent flux drive $X_{\boldsymbol{k}}$, the collisional dissipation $D_{\boldsymbol{k}}$ and the parallel streaming term $E_{\boldsymbol{k}}$ (which represents the mode conversion due to the parallel streaming in the sheared magnetic field [17]) are respectively given by,

$$S_{\boldsymbol{k}} = \sum_{\mathrm{s}} \left\langle \int dv^3 \frac{T_{\mathrm{s}} |\tilde{f}_{\mathrm{s}\boldsymbol{k}}|^2}{2F_{\mathrm{Ms}}} \right\rangle, \tag{5}$$

$$W_{\boldsymbol{k}} = \left\langle \left[\varepsilon_0 k_\perp^2 + \sum_{\mathrm{s}} \frac{e_{\mathrm{s}}^2 n_{\mathrm{s}}}{T_{\mathrm{s}}} \left(1 - \Gamma_{0\mathrm{s}\boldsymbol{k}}\right) \right] \frac{|\tilde{\phi}_{\boldsymbol{k}}|^2}{2} + \frac{k_\perp^2}{\mu_0} \frac{|\tilde{A}_{\parallel\boldsymbol{k}}|^2}{2} \right\rangle, \tag{6}$$

$$X_{\boldsymbol{k}} = \sum_{\mathrm{s}} \left[\frac{T_{\mathrm{s}} \Gamma_{\mathrm{s}\boldsymbol{k}}}{L_{n_{\mathrm{s}}}} + \frac{1}{L_{T_{\mathrm{s}}}} \left(Q_{\mathrm{s}\boldsymbol{k}} - \frac{3}{2} T_{\mathrm{s}} \Gamma_{\mathrm{s}\boldsymbol{k}} \right) \right], \tag{7}$$

$$D_{\boldsymbol{k}} = \mathrm{Re} \left[\left\langle \int dv^3 \left(\frac{T_{\mathrm{s}} \tilde{f}^*_{\mathrm{s}\boldsymbol{k}}}{F_{\mathrm{Ms}}} + e_{\mathrm{s}} J_{0\mathrm{s}\boldsymbol{k}} \tilde{\phi}^*_{\boldsymbol{k}} \right) C_{\mathrm{s}\boldsymbol{k}} \right\rangle \right], \tag{8}$$

$$E_{\boldsymbol{k}} = -\left\langle \int dv^3 \nabla_\parallel \left[\frac{v_\parallel F_{\mathrm{sM}}}{2T_{\mathrm{s}}} \left| \frac{T_{\mathrm{s}} \tilde{f}^*_{\mathrm{s}\boldsymbol{k}}}{F_{\mathrm{Ms}}} + e_{\mathrm{s}} J_{0\mathrm{s}\boldsymbol{k}} \tilde{\phi}_{\boldsymbol{k}} \right|^2 \right] \right\rangle, \tag{9}$$

with the particle and energy fluxes $\Gamma_{\mathrm{s}\boldsymbol{k}} = \mathrm{Re}[\langle \int dv^3 i k_y J_{0\mathrm{s}\boldsymbol{k}} (\tilde{\phi}^*_{\boldsymbol{k}} - v_\parallel \tilde{A}^*_{\parallel\boldsymbol{k}}) \tilde{f}_{\mathrm{s}\boldsymbol{k}} / B \rangle]$, $Q_{\mathrm{s}\boldsymbol{k}} = \mathrm{Re}[\langle \int dv^3 i k_y J_{0\mathrm{s}\boldsymbol{k}} (\tilde{\phi}^*_{\boldsymbol{k}} - v_\parallel \tilde{A}^*_{\parallel\boldsymbol{k}}) (m_{\mathrm{s}} v_\parallel^2/2 + \mu B) \tilde{f}_{\mathrm{s}\boldsymbol{k}} / B \rangle]$ and density and temperature scale lengths $L_{n_{\mathrm{s}}} = |\nabla \ln n_{\mathrm{s}}|^{-1}$, $L_{T_{\mathrm{s}}} = |\nabla \ln T_{\mathrm{s}}|^{-1}$. The last term $I_{\boldsymbol{k}}$ is the gyrokinetic entropy transfer term describing mode-to-mode coupling via the $\boldsymbol{E} \times \boldsymbol{B}$ and magnetic nonlinearities. The role of this term in nonlinear plasma turbulence is extensively investigated, e.g., on the entropy cascade [18, 19], zonal flow shearing [20], and magnetic stochastization [21]. The gyrokinetic entropy transfer is given by

$$I_{\boldsymbol{k}} = \sum_{\boldsymbol{p}} \sum_{\boldsymbol{q}} J^{\boldsymbol{p},\boldsymbol{q}}_{\boldsymbol{k}}, \tag{10}$$

where the triad transfer has a symmetric form [20],

$$J^{\boldsymbol{p},\boldsymbol{q}}_{\boldsymbol{k}} = \sum_{\mathrm{s}} \delta_{\boldsymbol{k}+\boldsymbol{p}+\boldsymbol{q},\boldsymbol{0}} \frac{\boldsymbol{b} \cdot \boldsymbol{p} \times \boldsymbol{q}}{2B} \times \mathrm{Re} \left[\left\langle \int dv^3 \left(\bar{\psi}_{\mathrm{s}\boldsymbol{p}} \tilde{g}_{\mathrm{s}\boldsymbol{q}} - \bar{\psi}_{\mathrm{s}\boldsymbol{q}} \tilde{g}_{\mathrm{s}\boldsymbol{p}} \right) \frac{T_{\mathrm{s}} \tilde{g}_{\mathrm{s}\boldsymbol{k}}}{F_{\mathrm{Ms}}} \right\rangle \right], \tag{11}$$

with the gyrophase-averaged generalized potential $\bar{\psi}_{\mathrm{s}\boldsymbol{k}} = J_{0\mathrm{s}\boldsymbol{k}} (\tilde{\phi}_{\boldsymbol{k}} - v_\parallel \tilde{A}_{\parallel\boldsymbol{k}})$ and the non-adiabatic part of the perturbed distribution function $\tilde{g}_{\mathrm{s}\boldsymbol{k}} = \tilde{f}_{\mathrm{s}\boldsymbol{k}} + e_{\mathrm{s}} J_{0\mathrm{s}\boldsymbol{k}} \tilde{\phi}_{\boldsymbol{k}} F_{\mathrm{Ms}} / T_{\mathrm{s}}$. The angular brackets $\langle \cdots \rangle$ denotes the average over the field aligned coordinate z. Under the coupling condition $\boldsymbol{k} + \boldsymbol{p} + \boldsymbol{q} = \boldsymbol{0}$, the triad transfer satisfies the symmetry $J^{\boldsymbol{p},\boldsymbol{q}}_{\boldsymbol{k}} = J^{\boldsymbol{q},\boldsymbol{p}}_{\boldsymbol{k}}$, the detailed balance $J^{\boldsymbol{p},\boldsymbol{q}}_{\boldsymbol{k}} + J^{\boldsymbol{k},\boldsymbol{p}}_{\boldsymbol{q}} + J^{\boldsymbol{q},\boldsymbol{k}}_{\boldsymbol{p}} = 0$, and if $\boldsymbol{k}$, $\boldsymbol{p}$ and $\boldsymbol{q}$ are parallel, $J^{\boldsymbol{p},\boldsymbol{q}}_{\boldsymbol{k}} = 0$. Therefore, possible combinations of the triad coupling $J^{\boldsymbol{p},\boldsymbol{q}}_{\boldsymbol{k}}$, $J^{\boldsymbol{k},\boldsymbol{p}}_{\boldsymbol{q}}$, $J^{\boldsymbol{q},\boldsymbol{k}}_{\boldsymbol{p}}$ are 2 givers and 1 taker $(-,-,+)$ or 1 giver and 2 takers $(-,+,+)$. For example, the negative triad transfer $J^{\boldsymbol{p},\boldsymbol{q}}_{\boldsymbol{k}}$ physically means that the entropy of the $\boldsymbol{k}$ mode is transferred to the $\boldsymbol{p}$ or $\boldsymbol{q}$ modes, while its direction is unknown until examining $J^{\boldsymbol{k},\boldsymbol{p}}_{\boldsymbol{q}}$ and $J^{\boldsymbol{q},\boldsymbol{k}}_{\boldsymbol{p}}$. Summing up contributions through all triad couplings, the total entropy transfer $I_{\boldsymbol{k}}$ describes the $\boldsymbol{k}$ mode is nonlinearly excited or damped. It is also noted

that, since $X_{k_y=0} = E_{k_y=0} = 0$ and $D_{\boldsymbol{k}}$ is a negative definite, the total transfer for zonal ($k_y = 0$) modes should be positive $I_{k_y=0} = -D_{k_y=0} > 0$ in the steady state.

2.2.1. Fluid approximation of gyrokinetic triad transfer The total entropy transfer, Eq. (10), can be rewritten as $I_{\boldsymbol{k}} = -\sum_{\rm s} {\rm Re}[\langle \int dv^3 N_{{\rm s}\boldsymbol{k}} T_{\rm s} \tilde{g}_{{\rm s}\boldsymbol{k}} / F_{\rm Ms} \rangle]$, and is easily evaluated with a small computational cost. Considering the implementation of the gyrokinetic triad transfer analysis, Eq. (11), however, one have to treat the combination of all Fourier modes with keeping 5D phase space information. Then, it demands extreme computations especially for multi-scale turbulence. To reduce the computational complexity, we consider a fluid approximation of the gyrokinetic triad transfer. One of possible approaches is the Hermite and Laguerre expansion (for $v_\parallel$ and μ, respectively) of the "gyrocenter-position" distribution function $\tilde{f}_{{\rm s}\boldsymbol{k}}$ [22]. An alternative way, which we employ here, is the expansion of the non-adiabatic part of the "particle-position" distribution function $J_{0{\rm s}\boldsymbol{k}} \tilde{g}_{{\rm s}\boldsymbol{k}}$,

$$J_{0{\rm s}\boldsymbol{k}} \tilde{g}_{{\rm s}\boldsymbol{k}} = \sum_{l=0}^{\infty} \sum_{m=0}^{\infty} \frac{M_{{\rm s}\boldsymbol{k}|l,m}}{l!} H_l(\bar{v}_\parallel) L_m(\bar{\mu}) F_{\rm Ms}, \tag{12}$$

$$M_{{\rm s}\boldsymbol{k}|l,m} = \int dv^3 H_l(\bar{v}_\parallel) L_m(\bar{\mu}) J_{0{\rm s}\boldsymbol{k}} \tilde{g}_{{\rm s}\boldsymbol{k}}, \tag{13}$$

where $\bar{v}_\parallel = v_\parallel / v_{\rm ts}$ and $\bar{\mu} = \mu B / T_{\rm s}$. We note that the Hermite and Laguerre polynomials with the Maxwellian weight function, $H_l(x) = (-1)^l \exp(x^2/2)(d/dx)^l \exp(-x^2/2)$ and $L_m(x) = \exp(x)/m!(d/dx)^m[x^n \exp(-x)]$, satisfy the orthogonality relations, $\int_{-\infty}^{\infty} dx H_l(x) H_n(x) \exp(-x^2/2) = l!\sqrt{2\pi}\delta_{l,n}$ and $\int_0^{\infty} dx L_m(x) L_n(x) \exp(-x) = \delta_{m,n}$. By defining fluid moments as

$$\tilde{n}_{{\rm s}\boldsymbol{k}} = \int dv^3 J_{0{\rm s}\boldsymbol{k}} f_{{\rm s}\boldsymbol{k}}, \tag{14}$$

$$\tilde{u}_{\parallel{\rm s}\boldsymbol{k}} = \int dv^3 v_\parallel J_{0{\rm s}\boldsymbol{k}} f_{{\rm s}\boldsymbol{k}}, \tag{15}$$

$$\tilde{p}_{\parallel{\rm s}\boldsymbol{k}} = \int dv^3 m_{\rm s} v_\parallel^2 J_{0{\rm s}\boldsymbol{k}} f_{{\rm s}\boldsymbol{k}}, \tag{16}$$

$$\tilde{p}_{\perp{\rm s}\boldsymbol{k}} = \int dv^3 \mu B J_{0{\rm s}\boldsymbol{k}} f_{{\rm s}\boldsymbol{k}}, \tag{17}$$

$$\tilde{q}_{\parallel\parallel{\rm s}\boldsymbol{k}} = \int dv^3 m_{\rm s} v_\parallel^3 J_{0{\rm s}\boldsymbol{k}} f_{{\rm s}\boldsymbol{k}}, \tag{18}$$

$$\tilde{q}_{\parallel\perp{\rm s}\boldsymbol{k}} = \int dv^3 v_\parallel \mu B J_{0{\rm s}\boldsymbol{k}} f_{{\rm s}\boldsymbol{k}}, \tag{19}$$

the expansion coefficients $M_{\mathrm{s}\boldsymbol{k}|l,m}$ up to the third order are given by

$$M_{\mathrm{s}\boldsymbol{k}|0,0} = \frac{\tilde{n}_{\mathrm{s}\boldsymbol{k}}}{n_\mathrm{s}} + \frac{e_\mathrm{s}\tilde{\phi}_{\boldsymbol{k}}}{T_\mathrm{s}}\Gamma_{0\mathrm{s}\boldsymbol{k}}, \tag{20}$$

$$M_{\mathrm{s}\boldsymbol{k}|1,0} = \frac{\tilde{u}_{\parallel\mathrm{s}\boldsymbol{k}}}{n_\mathrm{s} v_\mathrm{ts}}, \tag{21}$$

$$M_{\mathrm{s}\boldsymbol{k}|2,0} = \frac{\tilde{p}_{\parallel\mathrm{s}\boldsymbol{k}}}{n_\mathrm{s} T_\mathrm{s}} - \frac{\tilde{n}_{\mathrm{s}\boldsymbol{k}}}{n_\mathrm{s}}, \tag{22}$$

$$M_{\mathrm{s}\boldsymbol{k}|0,1} = -\frac{\tilde{p}_{\perp\mathrm{s}\boldsymbol{k}}}{n_\mathrm{s} T_\mathrm{s}} + \frac{\tilde{n}_{\mathrm{s}\boldsymbol{k}}}{n_\mathrm{s}} + \frac{e_\mathrm{s}\tilde{\phi}_{\boldsymbol{k}}}{T_\mathrm{s}} k_\perp^2 \rho_\mathrm{ts}^2 (\Gamma_{0\mathrm{s}\boldsymbol{k}} - \Gamma_{1\mathrm{s}\boldsymbol{k}}), \tag{23}$$

$$M_{\mathrm{s}\boldsymbol{k}|3,0} = \frac{\tilde{q}_{\parallel\parallel\mathrm{s}\boldsymbol{k}}}{n_\mathrm{s} T_\mathrm{s} v_\mathrm{ts}} - \frac{3\tilde{u}_{\parallel\mathrm{s}\boldsymbol{k}}}{n_\mathrm{s} v_\mathrm{ts}}, \tag{24}$$

$$M_{\mathrm{s}\boldsymbol{k}|1,1} = -\frac{\tilde{q}_{\parallel\perp\mathrm{s}\boldsymbol{k}}}{n_\mathrm{s} T_\mathrm{s} v_\mathrm{ts}} + \frac{\tilde{u}_{\parallel\mathrm{s}\boldsymbol{k}}}{n_\mathrm{s} v_\mathrm{ts}}, \tag{25}$$

where $\Gamma_{1\mathrm{s}\boldsymbol{k}} = I_1(k_\perp^2\rho_\mathrm{ts}^2)\exp(-k_\perp^2\rho_\mathrm{ts}^2)$. For evaluation of the triad transfer, velocity-space integrals of $J_{0\mathrm{s}\boldsymbol{p}}\tilde{\phi}_{\boldsymbol{p}}\tilde{g}_{\mathrm{s}\boldsymbol{q}}\tilde{g}_{\mathrm{s}\boldsymbol{k}}/F_\mathrm{Ms}$ and $v_\parallel J_{0\mathrm{s}\boldsymbol{p}}\tilde{A}_{\parallel\boldsymbol{p}}\tilde{g}_{\mathrm{s}\boldsymbol{q}}\tilde{g}_{\mathrm{s}\boldsymbol{k}}$ are required. Using Neumann's addition theorem for Bessel functions $J_{0\mathrm{s}\boldsymbol{p}} = J_{0\mathrm{s}\boldsymbol{q}}J_{0\mathrm{s}\boldsymbol{k}} + 2\sum_{n=1}^{\infty}(-1)^n J_{n\mathrm{s}\boldsymbol{q}}J_{n\mathrm{s}\boldsymbol{k}}\cos(n\theta_{\boldsymbol{q}\boldsymbol{k}})$, where $\boldsymbol{k}+\boldsymbol{p}+\boldsymbol{q}=0$ and $\theta_{\boldsymbol{q}\boldsymbol{k}}$ is the angle between $\boldsymbol{q}$ and $\boldsymbol{k}$, the integrals become

$$\begin{aligned}
&\int dv^3 \frac{J_{0\mathrm{s}\boldsymbol{p}}\tilde{\phi}_{\boldsymbol{p}}\tilde{g}_{\mathrm{s}\boldsymbol{q}}\tilde{g}_{\mathrm{s}\boldsymbol{k}}}{F_\mathrm{Ms}} = \tilde{\phi}_{\boldsymbol{p}}\int dv^3 \Bigg[J_{0\mathrm{s}\boldsymbol{q}}\tilde{g}_{\mathrm{s}\boldsymbol{q}}J_{0\mathrm{s}\boldsymbol{k}}\tilde{g}_{\mathrm{s}\boldsymbol{k}} \\
&+ 2\sum_{n=1}^{\infty}(-1)^n J_{n\mathrm{s}\boldsymbol{q}}\tilde{g}_{\mathrm{s}\boldsymbol{q}}J_{n\mathrm{s}\boldsymbol{k}}\tilde{g}_{\mathrm{s}\boldsymbol{k}}\cos(n\theta_{\boldsymbol{q}\boldsymbol{k}})\Bigg] \\
&\simeq \tilde{\phi}_{\boldsymbol{p}}\sum_l\sum_m \frac{n_\mathrm{s}}{l!} M_{\mathrm{s}\boldsymbol{q}|l,m}M_{\mathrm{s}\boldsymbol{k}|l,m},
\end{aligned} \tag{26}$$

$$\begin{aligned}
&\int dv^3 v_\parallel \frac{J_{0\mathrm{s}\boldsymbol{p}}\tilde{A}_{\parallel\boldsymbol{p}}\tilde{g}_{\mathrm{s}\boldsymbol{q}}\tilde{g}_{\mathrm{s}\boldsymbol{k}}}{F_\mathrm{Ms}} \simeq \\
&v_\mathrm{ts}\tilde{A}_{\parallel\boldsymbol{p}}\sum_l\sum_m \frac{n_\mathrm{s}}{l!}(M_{\mathrm{s}\boldsymbol{q}|l+1,m} + lM_{\mathrm{s}\boldsymbol{q}|l-1,m})M_{\mathrm{s}\boldsymbol{k}|l,m},
\end{aligned} \tag{27}$$

here we neglect $n > 0$ higher order terms for simplicity. As a result, the gyrokinetic triad transfer, Eq. (11), is approximated by the fluid moments

$$\begin{aligned}
J_{\boldsymbol{k}}^{\boldsymbol{p},\boldsymbol{q}} &\simeq J_{\boldsymbol{k}(f)}^{\boldsymbol{p},\boldsymbol{q}} \\
&= \sum_\mathrm{s}\delta_{\boldsymbol{k}+\boldsymbol{p}+\boldsymbol{q},\boldsymbol{0}}\frac{n_\mathrm{s}T_\mathrm{s}\boldsymbol{b}\cdot\boldsymbol{p}\times\boldsymbol{q}}{2B} \\
&\times \mathrm{Re}\Bigg[\sum_l\sum_m\Bigg\langle\{\tilde{\phi}_{\boldsymbol{p}}M_{\mathrm{s}\boldsymbol{q}|l,m} - \tilde{\phi}_{\boldsymbol{q}}M_{\mathrm{s}\boldsymbol{p}|l,m} \\
&- v_\mathrm{ts}\tilde{A}_{\parallel\boldsymbol{p}}(M_{\mathrm{s}\boldsymbol{q}|l+1,m} + lM_{\mathrm{s}\boldsymbol{q}|l-1,m}) \\
&+ v_\mathrm{ts}\tilde{A}_{\parallel\boldsymbol{q}}(M_{\mathrm{s}\boldsymbol{p}|l+1,m} + lM_{\mathrm{s}\boldsymbol{p}|l-1,m})\}\frac{M_{\mathrm{s}\boldsymbol{k}|l,m}}{l!}\Bigg\rangle\Bigg],
\end{aligned} \tag{28}$$

for the practical purpose we have employed fluid moments up to the third order, Eqs. (20) - (25). The fluid approximation significantly reduces the computational cost

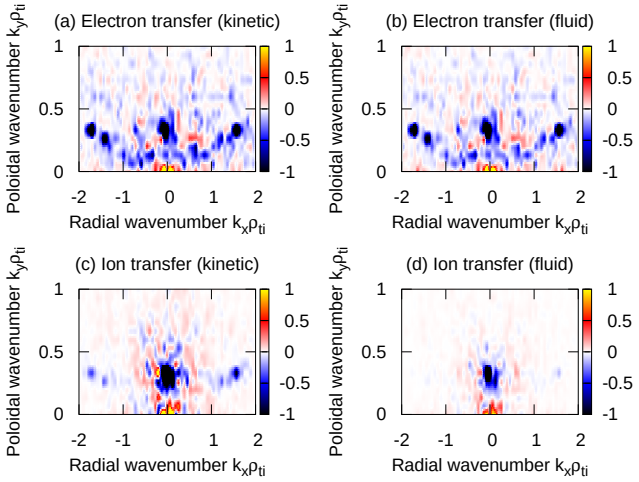

Figure 1. Comparison of gyrokinetic entropy transfer $I_{\boldsymbol{k}} = \sum_{\boldsymbol{p}} \sum_{\boldsymbol{q}} J^{\boldsymbol{p},\boldsymbol{q}}_{\boldsymbol{k}}$ and its fluid approximation $I_{\boldsymbol{k}(f)} = \sum_{\boldsymbol{p}} \sum_{\boldsymbol{q}} J^{\boldsymbol{p},\boldsymbol{q}}_{\boldsymbol{k}(f)}$, where $J^{\boldsymbol{p},\boldsymbol{q}}_{\boldsymbol{k}(f)}$ is given by Eq. (28) up to the third order (normalized by $n_0 T_{\rm i} v_{\rm ti} \rho_{\rm ti}^2 / R^3$). We have split the transfer into each species, (a)-(b) for electrons and (c)-(d) for ions. Positive (negative) transfer means that the mode $\boldsymbol{k}$ obtains (loses) its entropy via nonlinear mode coupling.

and memory. It only requires 3D data of the fluid moments of Eqs. (14) - (19) and electromagnetic potentials, and can be treated by post-processing.

Figure 1 plots the total entropy transfer evaluated by the gyrokinetic description or the fluid approximation by using the multi-scale turbulence data at the saturated state, where ion-scale fluctuations dominate as shown in Sec. 3. Regarding to the electron entropy transfer in Fig. 1 (a) and (b), the fluid approximation captures qualitative properties such as negative entropy transfer to the dominant ITG modes at $(k_x \rho_{\rm ti}, k_y \rho_{\rm ti}) \simeq (0, 0.3)$ and its twisted mode in the sheared magnetic geometry [23, 24] on the line of $k_x = \pm 2\pi \hat{s} k_y$, where $\hat{s}$ is the magnetic shear. It also satisfies the theoretical requirement on the positivity of entropy transfer to zonal modes. Unfortunately, the absolute value of the fluid approximation have differences of order unity from the gyrokinetic one, and thus is not applicable for quantitative evaluations of nonlinear couplings. Fluid approximation of the ion transfer also shows qualitative agreement with gyrokinetic one at the low wave number region, although the transfer at $k\rho_{\rm ti} > 1$ is underestimated [See Fig. 1 (c) and (d)]. The errors in the fluid approximation originate from (i) the truncation of the fluid moments and (ii) the finite-Larmor-radius correction of neglecting higher-order terms in the expansion of the Bessel function, Eqs. (26), (27). The latter seems to underestimate the transfer at high wave number region $k\rho_{\rm ts}$. As a consequence, Fig. 1 demonstrates a qualitative applicability of the fluid approximation.

2.2.2. Sub-space transfer analysis From the ETG/ITG turbulence simulation results, ETG is strongly distorted by ITG turbulence and there is no coherent structure at electron scales. To analyze collective behaviors of electron-scale turbulence, we here define sub-space transfer analysis technique. We divide the wave-number space $\Omega = \{\boldsymbol{k}\}$ into several sub-spaces Ω_k, where the union of all sub-spaces constructs the

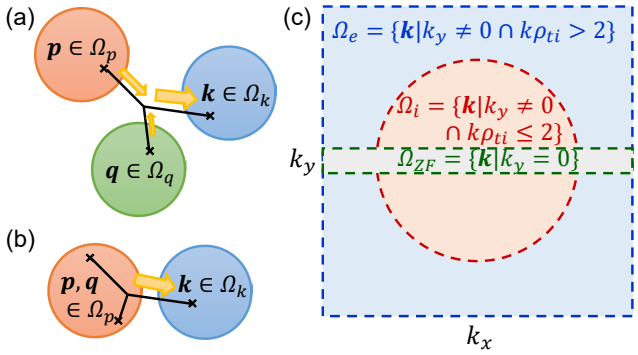

Figure 2. (a) Schematic picture of the sub-space transfer $J_{\Omega_k}^{\Omega_p,\Omega_q}$, (b) Example of $J_{\Omega_k}^{\Omega_p,\Omega_p} \neq 0$, and (c) Split of the wave number space into zonal modes $\Omega_{\rm ZF} = \{\boldsymbol{k} \mid k_y = 0\}$, ion-scale modes $\Omega_i = \{\boldsymbol{k} \mid |k_y \neq 0 \cap k\rho_{\rm ti} \leq 2\}$, and electron-scale modes $\Omega_e = \{\boldsymbol{k} \mid k_y \neq 0 \cap k\rho_{\rm ti} > 2\}$.

whole wave-number space $\cup_k \Omega_k = \Omega$ and the each intersections are empty $\Omega_k \cap \Omega_p = \emptyset$. Taking the sum over $\boldsymbol{k}$ in a sub-space, the sub-space entropy balance

$$\frac{d}{dt}(S_{\Omega_k} + W_{\Omega_k}) = X_{\Omega_k} + D_{\Omega_k} + E_{\Omega_k} + I_{\Omega_k}, \tag{29}$$

the nonlinear entropy transfer

$$I_{\Omega_k} = \sum_{\Omega_p} \sum_{\Omega_q} J_{\Omega_k}^{\Omega_p,\Omega_q}, \tag{30}$$

and the sub-space transfer

$$J_{\Omega_k}^{\Omega_p,\Omega_q} = \sum_{\boldsymbol{k}\in\Omega_k} \sum_{\boldsymbol{p}\in\Omega_p} \sum_{\boldsymbol{q}\in\Omega_q} J_{\boldsymbol{k}}^{\boldsymbol{p},\boldsymbol{q}}, \tag{31}$$

are respectively defined, where $\sum_{\Omega_k}$ means the summation over all sub-spaces and $\sum_{\boldsymbol{k}\in\Omega_k}$ means the summation over all $\boldsymbol{k}$ being an element of Ω_k. Thus, $\sum_{\boldsymbol{k}\in\Omega} = \sum_{\Omega_k}\sum_{\boldsymbol{k}\in\Omega_k}$. The sub-space transfer measures the entropy gain for the modes in the sub-space Ω_k via nonlinear triad interactions with the modes in Ω_p and Ω_q [schematically shown in Fig. 2 (a)] and preserves some mathematical properties such as the symmetry $J_{\Omega_k}^{\Omega_p,\Omega_q} = J_{\Omega_k}^{\Omega_q,\Omega_p}$ and the detailed balance $J_{\Omega_k}^{\Omega_p,\Omega_q} + J_{\Omega_q}^{\Omega_k,\Omega_p} + J_{\Omega_p}^{\Omega_q,\Omega_k} = 0$ (and especially the self-conservation $J_{\Omega_k}^{\Omega_k,\Omega_k} = 0$) in the same manner as the triad transfer. A property different from the triad transfer is that $J_{\Omega_k}^{\Omega_p,\Omega_p} \neq 0$ if $\Omega_p \neq \Omega_k$, since $\boldsymbol{p} \in \Omega_p$ and $\boldsymbol{q} \in \Omega_p$ can interact with $\boldsymbol{k} \in \Omega_k$ [Fig. 2 (b)]. The sub-space transfer analysis is regarded as a natural extension of a shell-to-shell transfer (often used for the analysis of neutral fluids and applied for some studies on plasma turbulence), where sub-spaces are chosen to be concentric shells $\Omega_n = \{\boldsymbol{k} \mid |k - n\Delta| < \Delta/2\}$ with the width Δ, and then, $\sum_{\Omega_q} J_{\Omega_k}^{\Omega_p,\Omega_q}$ is regarded as the transfer between the shells Ω_k and Ω_p. Although the shell-to-shell transfer is essentially appropriate for homogeneous turbulence, the sub-space transfer allows flexible analysis of interactions among arbitrary sub sets of wave-number space. It is desirable for the analysis of

plasma turbulence which is often anisotropic especially in case with the strong zonal flows. Indeed, in the following section the wave-number space is divided into zonal modes $\Omega_{\rm ZF} = \{\boldsymbol{k} \mid k_y = 0\}$, ion-scale modes $\Omega_i = \{\boldsymbol{k} \mid |k_y \neq 0 \cap k\rho_{\rm ti} \leq 2\}$, and electron-scale modes $\Omega_e = \{\boldsymbol{k} \mid k_y \neq 0 \cap k\rho_{\rm ti} > 2\}$, as drawn in Fig. 2 (c).

The computational cost of the sub-space transfer can be reduced by using the Fast Fourier Transform algorithm (FFT), when the number of sub-spaces are not large. The wave-number-space filter

$$G_{\boldsymbol{k}}^{\Omega_k} = \begin{cases} 1 & (\boldsymbol{k} \in \Omega_k) \\ 0 & (\boldsymbol{k} \notin \Omega_k) \end{cases} \tag{32}$$

leads to the expression $\sum_{\boldsymbol{k}\in\Omega_k} = \sum_{\boldsymbol{k}} G_{\boldsymbol{k}}^{\Omega_k}$, and therefore sub-space transfer can be expanded as

$$J_{\Omega_k}^{\Omega_p,\Omega_q} = \sum_{\rm s} {\rm Re}\left[\left\langle \int dv^3 \sum_{\boldsymbol{k}} \frac{T_{\rm s}(G_{\boldsymbol{k}}^{\Omega_k}\tilde{g}_{{\rm s}\boldsymbol{k}})}{F_{\rm Ms}} \mathcal{N}_{{\rm s}\boldsymbol{k}}^{\Omega_p,\Omega_q} \right\rangle\right], \tag{33}$$

$$\begin{aligned} \mathcal{N}_{{\rm s}\boldsymbol{k}}^{\Omega_p,\Omega_q} &= \sum_{\boldsymbol{p}}\sum_{\boldsymbol{q}} \delta_{\boldsymbol{k}+\boldsymbol{p}+\boldsymbol{q},\boldsymbol{0}} \frac{\boldsymbol{b}\cdot\boldsymbol{p}\times\boldsymbol{q}}{2B} \\ &\times \left(G_{\boldsymbol{p}}^{\Omega_p}\bar{\psi}_{{\rm s}\boldsymbol{p}} G_{\boldsymbol{q}}^{\Omega_q}\tilde{g}_{{\rm s}\boldsymbol{q}} - G_{\boldsymbol{q}}^{\Omega_q}\bar{\psi}_{{\rm s}\boldsymbol{q}} G_{\boldsymbol{p}}^{\Omega_p}\tilde{g}_{{\rm s}\boldsymbol{p}}\right), \end{aligned} \tag{34}$$

Therefore, after the preparation of the filtered functions $G_{\boldsymbol{k}}^{\Omega_k}\bar{\psi}_{{\rm s}\boldsymbol{k}}$ and $G_{\boldsymbol{k}}^{\Omega_k}\tilde{g}_{{\rm s}\boldsymbol{k}}$, the convolution in Eq. (34) is calculated by using FFT with a reduced computational cost of the order of $N \log N$.

3. Results

Using the entropy transfer analysis techniques, we here investigated nonlinear interactions in multi-scale ETG/ITG turbulence. The following simulation data are the same as those in our previous publication [11], where plasma parameters are set to be the so-called cyclone base case parameters with employing realistic proton-to-electron mass ratio $m_{\rm i}/m_{\rm e} = 1836$ and β value (2%). A large number of grid points are employed to resolve electron and ion scales simultaneously.

3.1. Turbulent fluctuations and associated transport

At the beginning, we briefly describe time evolution of a multi-scale ETG/ITG turbulence simulation. Figure 3 shows snapshots of the electrostatic potential fluctuations in the bad curvature region ($z = 0$). Starting with almost quiescent initial conditions, the high-growth-rate ETG modes rapidly grow up. Saturated profile in Fig. 3 (a) demonstrate the appearance of radially elongated eddies, called as streamers [25]. After that, in the presence of ETG turbulence, the ITG modes linearly grow up in Fig. 3 (b). The most unstable ITG has the wavenumber $(k_x\rho_{\rm ti}, k_y\rho_{\rm ti}) = (0, 0.33)$ or equivalently the poloidal wavelength $\lambda_y = 18.8\rho_{\rm ti}$. It is also found that passing electrons tend to elongate the ITG mode structure in parallel direction and create twisted structures in the presence of magnetic shear. The radial wavenumber of the twisted mode is $k_x = 2\pi\hat{s}k_y = 1.6\rho_{\rm ti}^{-1}$ (or equivalently $\lambda_x = 3.8\rho_{\rm ti}$) for $k_y\rho_{\rm ti} = 0.33$ and $\hat{s} = 0.78$. This corresponds to the fine radial structures observed in Fig. 3 (b). Finally

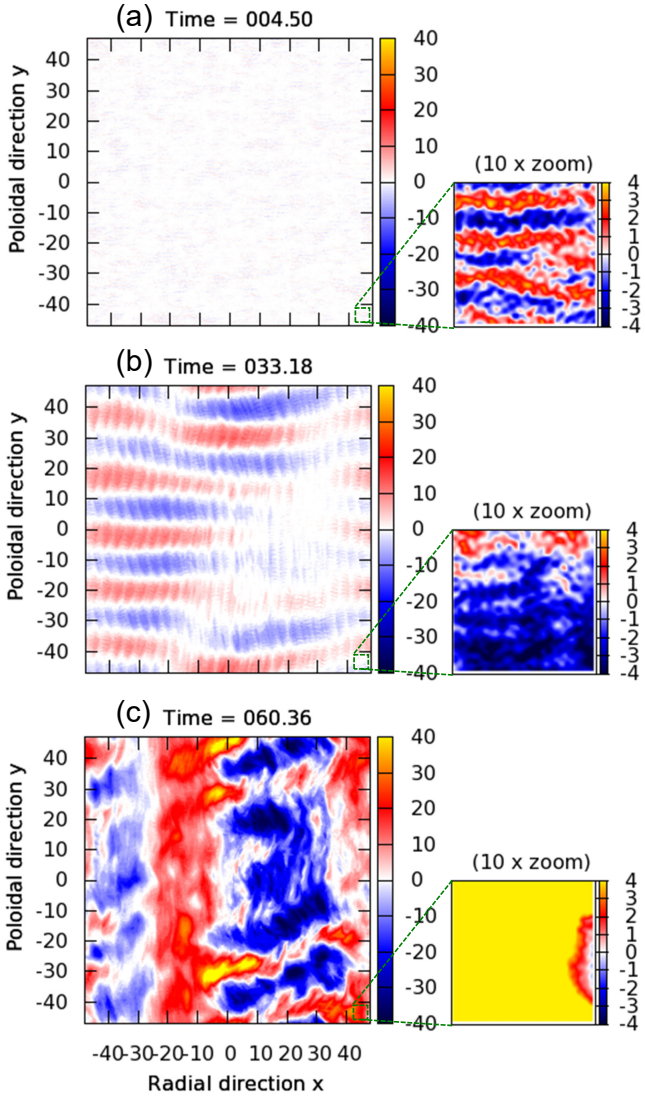

Figure 3. Snapshots of the electrostatic potential fluctuations $\tilde{\phi}$ [normalized by $T_{\rm i}\rho_{\rm ti}/(eR)$] at the flux-tube mid-plane $z = 0$ (bad curvature region). There are three time slices: (a) ETG-dominant regime at $t = 4.5R/v_{\rm ti}$, (b) linear growth of ITG at $t = 33.18R/v_{\rm ti}$, and (c) a quasi-steady state at $t = 60.36R/v_{\rm ti}$. Ten-times magnified pictures are also drawn to see electron scales.

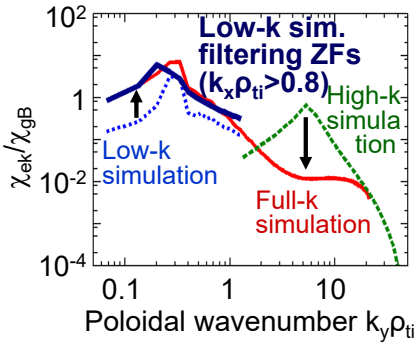

Figure 4. Electron energy diffusivity spectrum $\chi_{e\boldsymbol{k}}$ as a function of the poloidal wave number, obtained from a full-k simulation resolving multi-scale ETG/ITG turbulence (a solid red line), single-scale simulations resolving only electron-scale high-k modes (a dashed green line) or ion-scale low-k modes (a dotted blue line). Transport levels in a low-k simulation filtering out $k_x\rho_{\rm ti} > 0.8$ zonal fluctuations is also plotted (a thick blue line).

the growth of ITG instability is also saturated, and one finds a quasi-steady state of multi-scale ETG/ITG turbulence shown in Fig. 3 (c), where ITG-driven turbulent structures are dominant, and the electron-scale streamers almost disappear. (We note that there are reports that electron-scale streamers can locally survive against the background larger-scale ITG turbulence when employing marginal ITG parameters [7, 9].) The ITG turbulence generates various size of eddies and the large-scale zonal flows characterized by zero poloidal wave number $k_y = 0$. From the figure, its radial scale is $k_x\rho_{\rm ti} \simeq 0.13$ or equivalently $\lambda_x \simeq 48\rho_{\rm ti}$. One also finds $k_y\rho_{\rm ti} \simeq 0.33$ or lower-wave-number eddies and associated fine radial structures.

From this turbulence data, electron energy diffusivity spectrum is calculated by $\chi_{e\boldsymbol{k}} = Q_{e\boldsymbol{k}} L_{T_{\rm e}}/(n_0 T_{\rm e})$, as shown in Fig. 4. The normalization is in the ion gyro-Bohm unit $\chi_{\rm gB} = v_{\rm ti}\rho_{\rm ti}^2/R$. As ITG turbulence dominates in a quasi-steady state, ion-scale fluctuations are responsible for a large amount of electron energy transport, peaking around $(k_x, k_y) = (0, 0.3\rho_{\rm ti})$. Comparing the multi-scale (full-k) simulation results to other single-scale ones resolving only electron or ion scales (high-k and low-k), one finds a significant reduction of the electron-scale transport, and at the same time, an enhancement of the ion-scale transport in the multi-scale ETG/ITG turbulence. The results clearly demonstrate the mutual cross-scale interactions. In Fig. 4, an ion-scale simulation result with artificially filtering out high-wave-number ($k_x\rho_{\rm ti} > 0.8$) zonal flows is also plotted. The result shows a clear enhancement of transport level in comparison to the nominal low-k simulation. This point will be discussed in Sec. 3.3.

Field energy spectrum in Fig. 5 also shows suppression of electron-scale turbulence and enhancement of ion-scale turbulence in a multi-scale ETG/ITG turbulence simulation. The plot includes zonal components having zero poloidal wave number $k_y = 0$. In consistent with Fig. 3, a single-scale ETG turbulence simulation (high-k) shows weak zonal flow generation and a distinct peak of streamers, while strong zonal flows are driven in single-scale ITG and multi-scale ETG/ITG turbulence simulations (low-k and full-k). It should be noted that total field energy is different by a factor of two, $\int W_k dk_y/(n_0 T_{\rm i}\rho_{\rm ti}^2/R^2) = 15.7$ and 30.8 for low-k and full-k simulations, but the energy of $k_y = 0$ zonal modes have only little change. Since zonal

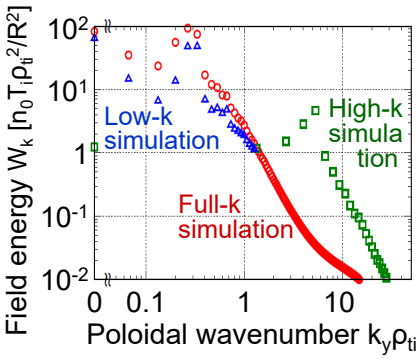

Figure 5. Field energy spectrum $W_{\boldsymbol{k}}$ as a function of the poloidal wave number, obtained from a full-k simulation resolving multi-scale ETG/ITG turbulence (circular dots), single-scale simulations resolving only electron-scale high-k modes (square dots) or ion-scale low-k modes (triangle dots).

modes are driven by the nonlinear entropy transfer from non-zonal modes, this means that generation of zonal modes becomes inefficient in the presence of electron-scale turbulence.

3.2. The $i \to e$ interaction

One of key questions we should address is: how does ion-scale turbulence suppress electron-scale streamers? The answer is the shearing of streamers by short-wavelength ITG eddies as explained in this subsection.

To evaluate cross-scale effects on a streamer, we have applied the detailed triad transfer analysis using the fluid approximation for a typical wave number of a streamer $\boldsymbol{k} = (0, 4.4\rho_{\rm ti}^{-1})$, as plotted in Fig. 6. For convenience, we again explain its physical meaning. The triad transfer function having six-dimensional dependence $(k_x, k_y, p_x, p_y, q_x, q_y)$ can be reduced to a two-dimensional function by imposing the resonant condition $\boldsymbol{k}+\boldsymbol{p}+\boldsymbol{q}=0$ and choosing a fixed $\boldsymbol{k}$. Then, $J_{\boldsymbol{k}}^{\boldsymbol{p},\boldsymbol{q}}(p_x, p_y)$, plotted as a function of $\boldsymbol{p}$, denotes the entropy gain of the analyzed mode $\boldsymbol{k}$ through the coupling with $\boldsymbol{p}$ (and $\boldsymbol{q} = -\boldsymbol{k}-\boldsymbol{p}$). On the other hand, $J_{\boldsymbol{p}}^{\boldsymbol{q},\boldsymbol{k}}(p_x, p_y)$ describes the gains of $\boldsymbol{p}$ modes through the coupling with the analyzed mode $\boldsymbol{k}$ (and $\boldsymbol{q}$). Then, Fig. 6 (a) shows that the analyzed $\boldsymbol{k} = (0, 4.4\rho_{\rm ti}^{-1})$ streamer couples with various modes in wide wave number range. Distinctive positive values of $J_{\boldsymbol{k}}^{\boldsymbol{p},\boldsymbol{q}}$ around $p_y \simeq -0.4\rho_{\rm ti}^{-1}$ and $p_y \simeq -4.0\rho_{\rm ti}^{-1}$ satisfying the resonant condition mean that the analyzed streamer obtains entropy through the coupling with these modes. On the other hand, negative values of $J_{\boldsymbol{k}}^{\boldsymbol{p},\boldsymbol{q}}$ around $p_y \simeq 0.4\rho_{\rm ti}^{-1}$ and $p_y \simeq -4.8\rho_{\rm ti}^{-1}$ means that entropy of the analyzed streamer is transferred to those modes. The above entropy giver and taker are clarified in Fig. 6 (b). The modes around $p_y \simeq -4.0\rho_{\rm ti}^{-1}$ (or $p_y \simeq -4.8\rho_{\rm ti}^{-1}$) mainly lose (or obtain) entropy via the coupling with the analyzed streamer of the mode $\boldsymbol{k}$, while the other modes have little loss or gain. This observation is consistent with the detailed balance $J_{\boldsymbol{k}}^{\boldsymbol{p},\boldsymbol{q}} + J_{\boldsymbol{q}}^{\boldsymbol{k},\boldsymbol{p}} + J_{\boldsymbol{p}}^{\boldsymbol{q},\boldsymbol{k}} = 0$, i.e., the analyzed $k_y \simeq 4.4\rho_{\rm ti}^{-1}$ streamer obtains the entropy ($J_{\boldsymbol{k}}^{\boldsymbol{p},\boldsymbol{q}} > 0$) from the modes $p_y \simeq -4.0\rho_{\rm ti}^{-1}$ ($J_{\boldsymbol{p}}^{\boldsymbol{q},\boldsymbol{k}} < 0$), where the coupled modes $q_y = -k_y - p_y \simeq -0.4\rho_{\rm ti}^{-1}$ acts like a mediator ($J_{\boldsymbol{q}}^{\boldsymbol{k},\boldsymbol{p}} \simeq 0$). Similarly, the entropy of the analyzed $k_y \simeq 4.4\rho_{\rm ti}^{-1}$ streamer is transferred to the modes $p_y \simeq -4.8\rho_{\rm ti}^{-1}$ via the copling with $q_y = -k_y - p_y \simeq 0.4\rho_{\rm ti}^{-1}$ ($-J_{\boldsymbol{k}}^{\boldsymbol{p},\boldsymbol{q}} \simeq J_{\boldsymbol{p}}^{\boldsymbol{q},\boldsymbol{k}} > 0 \simeq J_{\boldsymbol{q}}^{\boldsymbol{k},\boldsymbol{p}}$). We have

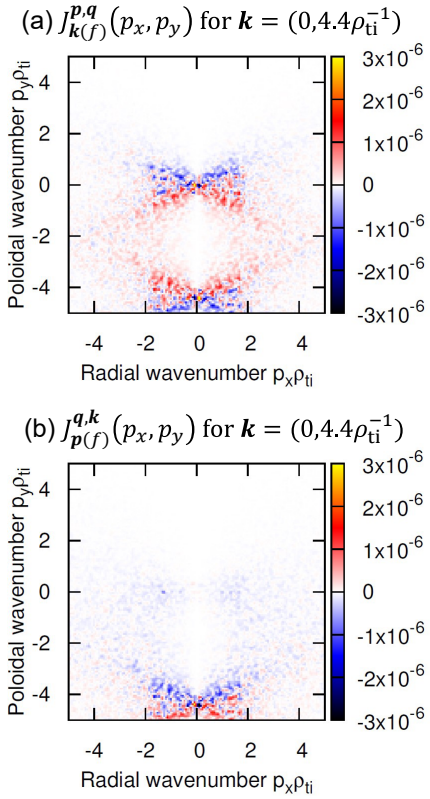

Figure 6. Analysis of the triad transfer for a streamer based on the fluid approximation (normalized by $n_0T_{\rm i}v_{\rm ti}\rho_{\rm ti}^2/R^3$). (a) $J^{\boldsymbol{p},\boldsymbol{q}}_{\boldsymbol{k}(f)}$ for $\boldsymbol{k}=(0,4.4\rho_{\rm ti}^{-1})$ is plotted as a function of $\boldsymbol{p}$, which represents the entropy gain of the fixed mode $\boldsymbol{k}$ through the coupling with $\boldsymbol{p}$. (b) $J^{\boldsymbol{q},\boldsymbol{k}}_{\boldsymbol{p}(f)}$ for $\boldsymbol{k}=(0,4.4\rho_{\rm ti}^{-1})$ is plotted as a function of $\boldsymbol{p}$, which represents the entropy gain of $\boldsymbol{p}$ through the coupling with the fixed mode $\boldsymbol{k}$.

checked the triad transfer functions not only of the mode $\boldsymbol{k}=(0,4.4\rho_{\rm ti}^{-1})$ but also of some other modes around wave-number range of the typical ETG turbulence, and observed similar entropy transfers through the coupling with ion-scale eddies.

Although strong low-wave-number zonal flows having $k_x\rho_{\rm ti}=0.13$ are observed in the previous subsection, its contribution on an electron-scale streamer is not dominant. The relevant wave number for cross-scale coupling between ITG turbulence and ETG streamers are clearly shown in Fig. 7, where positive/negative contributions on the analyzed streamer are separately shell integrated in the wave number space,

$$J^{\boldsymbol{p},\boldsymbol{q}}_{\boldsymbol{k}(+)}(p_\perp)=\frac{1}{\Delta p}\sum_{|p_\perp-p'_\perp|<\Delta p/2}J^{\boldsymbol{p}',\boldsymbol{q}}_{\boldsymbol{k}}(p'_x,p'_y)\left(\text{for } J^{\boldsymbol{p}',\boldsymbol{q}}_{\boldsymbol{k}}\geq 0\right), \tag{35}$$

$$J^{\boldsymbol{p},\boldsymbol{q}}_{\boldsymbol{k}(-)}(p_\perp)=\frac{1}{\Delta p}\sum_{|p_\perp-p'_\perp|<\Delta p/2}J^{\boldsymbol{p}',\boldsymbol{q}}_{\boldsymbol{k}}(p'_x,p'_y)\left(\text{for } J^{\boldsymbol{p}',\boldsymbol{q}}_{\boldsymbol{k}}< 0\right), \tag{36}$$

with a shell width of Δp. With the consideration of the detailed balance, the positive (or negative) contributions show that the analyzed streamer obtains from (loses to)

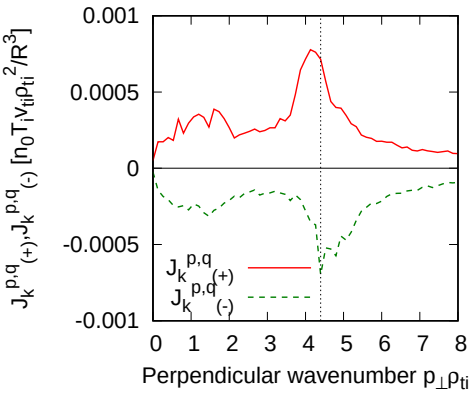

Figure 7. Shell-integrated triad transfer [from Fig. 6 (a)] with separating positive and negative contributions, $J^{\boldsymbol{p},\boldsymbol{q}}_{\boldsymbol{k}(+)}(p_\perp)$ and $J^{\boldsymbol{p},\boldsymbol{q}}_{\boldsymbol{k}(-)}(p_\perp)$ defined in Eqs.(35), (36) (where $\Delta p = 0.13\rho_{\rm ti}^{-1}$). The analyzed wave number of the streamer $|\boldsymbol{k}| = 4.4\rho_{\rm ti}^{-1}$ is also plotted by a dotted line as a reference.

the neighboring-wave-number modes through the coupling with ion-scale turbulence. The ion-scale turbulence works as a mediator, and eddies around $p_\perp\rho_{\rm ti} \simeq 1$ are more effective than low-wave-number zonal flows at $p_\perp\rho_{\rm ti} \simeq 0.13$.

From the observations in this section, we now draw a physical picture of suppression of electron-scale streamers by ion-scale turbulence as the $i \to e$ interaction. The ITG-driven ion-scale turbulence generates not only long-wave-length zonal flows but also involves large and small scale eddies. The long-wave-length zonal flows does not effectively act on electron-scale streamers because of separation of spatio-temporal scales. On the other hand, relatively short-wave-length ITG eddies having $k_\perp\rho_{\rm ti} \simeq 1$ easily interact with electron-scale streamers. They are still larger than electron scales and act like shear flows, tilting the electron-scale streamers and suppressing them. Then, electron scales are governed by a normal cascade, i.e., the entropy is transferred from the lower-wave-number modes to the higher-wave-number modes through the coupling with short-wave-length ITG eddies.

3.3. The $e \to i$ interaction

The second key question on the cross-scale interactions is: how does electron-scale turbulence enhance ion-scale transport? The key player is short-wave-length zonal flows which are created by the ITG modes with kinetic electrons, and damped by electron-scale turbulence, as explained in this subsection.

In the previous subsection it is revealed that electron scales are governed by a normal cascade. Therefore, the enhancement of the ion scale transport is not attributed to the inverse energy cascade from electron to ion scales. Obtaining a hint from the observation of inefficient zonal mode generation in a multi-scale ETG/ITG turbulence simulation, we focus on the entropy transfer to zonal modes. Ion-scale and electron-scale contributions are separately evaluated by using the sub-scape transfer analysis technique Eq. (31) with a fluid approximation, where the wave-number space is split into sub-spaces as shown in Fig. 2 (c). Fig. 8 shows radial wave number spectra of the entropy transfer to zonal modes, where the ion/electron entropy transfer

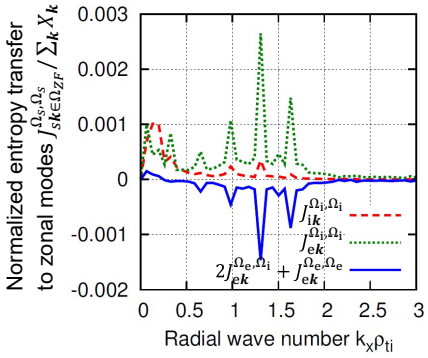

Figure 8. Sub-space transfer to zonal modes (normalized by the turbulent flux drive term $\sum_{\boldsymbol{k}} X_{\boldsymbol{k}}$), where $\Omega_{\rm ZF}$ is further split into each mode, and electron and ion entropy transfers are individually evaluated as $J^{\Omega_p,\Omega_q}_{\Omega_k} = \sum_{\rm s} J^{\Omega_p,\Omega_q}_{{\rm s}\Omega_k}$. The dashed red line shows the ion entropy transfer caused by ion-scale fluctuations $J^{\Omega_i,\Omega_i}_{{\rm i}\boldsymbol{k}\in\Omega_{\rm ZF}}$, while the dotted green and solid blue lines respectively represent the electron entropy transfer caused by ion-scale fluctuations and by electron-scale contributions, $J^{\Omega_i,\Omega_i}_{{\rm e}\boldsymbol{k}\in\Omega_{\rm ZF}}$ and $2J^{\Omega_e,\Omega_i}_{{\rm e}\boldsymbol{k}\in\Omega_{\rm ZF}} + J^{\Omega_e,\Omega_e}_{{\rm e}\boldsymbol{k}\in\Omega_{\rm ZF}}$.

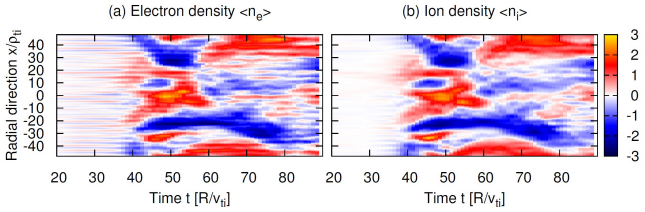

Figure 9. Time-space profile of the flux-surface averaged gyrocenter density (a) of electrons $\langle\tilde{n}_{\rm e}\rangle$ and (b) of ions $\langle\tilde{n}_{\rm s}\rangle$ (normalized by $n_0\rho_{\rm ti}/R$).

caused by the ion-scale/electron-scale turbulence is plotted. The ion entropy transfer from electron scales ($2J^{\Omega_e,\Omega_i}_{{\rm i}\boldsymbol{k}\in\Omega_{\rm ZF}} + J^{\Omega_e,\Omega_e}_{{\rm i}\boldsymbol{k}\in\Omega_{\rm ZF}}$) is negligibly small and is omitted. The ion entropy is transferred from ion-scale fluctuations to low-wave-number zonal modes at $k_x\rho_{\rm ti} \simeq 0.13$, as represented by $J^{\Omega_i,\Omega_i}_{{\rm i}\boldsymbol{k}\in\Omega_{\rm ZF}}$ which may be casually referred to the contribution from *ITG*. On the other hand, the electron entropy transfer caused by ion-scale fluctuations $J^{\Omega_i,\Omega_i}_{{\rm e}\boldsymbol{k}\in\Omega_{\rm ZF}}$, which corresponds to the contribution from *electron response in ITG*, drives not only the low-wave-number zonal modes but also relatively high-wave-number zonal modes at $k_x\rho_{\rm ti} = 1.3$ or 1.6. Their wave numbers correspond to the twisted mode in the sheared magnetic geometry $k_x\rho_{\rm ti} = 2\pi\hat{s}k_y\rho_{\rm ti} = 1.3$ or 1.6 for $k_y\rho_{\rm ti} = 0.26$ and 0.33, which are dominant poloidal wave numbers of the ITG turbulence. As recently discussed in the literature [24], passing kinetic electrons in ion-scale turbulence tend to elongate the mode structure in the parallel direction and in turn create radially-twisted structures. The nonlinear coupling with these radially-twisted modes drives high-wave-number zonal modes, which have non-negligible impact on turbulent transport. Supplementally, flux-surface averaged gyrocenter densities of electrons and ions in a multi-scale ETG/ITG turbulence simulation are plotted in Fig. 9, which shows the existence of high-wave-number zonal components of

the electron gyrocenter density. High-wave-number zonal flows are formed through the balance of the zonal electron gyrocenter density and the ion polarization. The electron entropy transfer caused by electron-scale turbulence $2J^{\Omega_e,\Omega_i}_{\mathrm{e}\boldsymbol{k}\in\Omega_{\mathrm{ZF}}}+J^{\Omega_e,\Omega_e}_{\mathrm{e}\boldsymbol{k}\in\Omega_{\mathrm{ZF}}}$, shown in Fig. 8 (a solid blue line), clearly demonstrates the damping effect on relatively high-wave-number zonal modes at $k_x\rho_{\mathrm{ti}}>1$ due to the electron-scale turbulence, while the effects on the low-wave-number zonal modes around $k_x\rho_{\mathrm{ti}}<0.5$ are negligibly small. We have also checked the impact of the high-wave-number zonal flows by conducting a single-scale ITG simulation with artificially filtering out the high-wave-number zonal flows, i.e., $\tilde{\phi}_{\boldsymbol{k}}=0$ for $k_y=0$ and $k_x\rho_{\mathrm{ti}}>0.8$. The result in Fig. 4 shows the enhancement of ion-scale transport levels by neglecting the high-wave-number zonal modes. The high-wave-number zonal flows have shearing rate comparable to low-wave-number zonal flows and affect ITG turbulence as discussed in [24].

From the above observation, we discuss a physical mechanism of the enhancement of ion-scale transport by electron-scale turbulence as the $e\to i$ interaction. Ion-scale ITG turbulence produces not only long-wave-length zonal flows but also short-wave-length ones. In the presence of kinetic electrons, mode structures of ITG elongate in the parallel direction and generate radially short-wave-length fluctuations/zonal flows in a sheared magnetic geometry. The short-wave-length zonal flows sustained by electron density fluctuations are disturbed by electron-scale turbulence. In other words, without kinetic electron response in ITG, there is no electron-scale contribution to the ion scale, since it will be averaged out by ion gyromotion. The damping effect of electron-scale turbulence on short-wave-length zonal flows reduces the zonal flow shearing, in turn, enhances the ion-scale transport.

4. Summary and discussion

We have carried out multi-scale ETG/ITG gyrokinetic simulations and investigated the physical mechanisms of cross-scale interactions by means of the fluid approximation of triad transfer analysis and the sub-space transfer analysis technique. First, a suppression mechanism of electron-scale turbulence by ion-scale turbulence (called as the $i\to e$ interaction) is examined in detail by using the triad transfer analysis on electron-scale streamers. Relatively short-wave-length eddies $k_\perp\rho_{\mathrm{ti}}\simeq 1$ caused by the ITG turbulence acts like shear flows on the electron-scale steamers and suppresses them. Then, the electron scale is governed by the normal cascade via the coupling with relatively short-wave-length ITG eddies. Second, an enhancement mechanism of ion-scale turbulence by electron-scale turbulence (called as the $e\to i$ interaction) is investigated by using the sub-space transfer analysis, where ion-scale and electron-scale contributions to zonal flow generation/damping are split. It is revealed that short-wave-length zonal flows $k_x\rho_{\mathrm{ti}}\simeq 1$ generated by the ITG turbulence with kinetic electrons are effectively damped by the electron-scale turbulence. As a result, reduction of zonal flow shear by the electron-scale turbulence enhances the ion-scale transport.

The above discussion is schematically summarized in Fig. 10. According to a single-scale turbulence paradigm, ion-scale turbulence (ITGs) at $k\rho_{\mathrm{i}}<1$ produces long-wave-length zonal flows (Low-k ZFs), of which the shearing motion suppresses ITGs. It is supposed to be independent of electron-scale turbulence (ETGs, Streamers) at $k\rho_{\mathrm{i}}\gg 1$. On the other hand, in a multi-scale paradigm, there are cross-scale interactions between electron and ion scales. First, ITG turbulence generates short-wave-length eddies (High-k Eddies) at $k\rho_{\mathrm{i}}\simeq 1$, which suppresses electron-scale

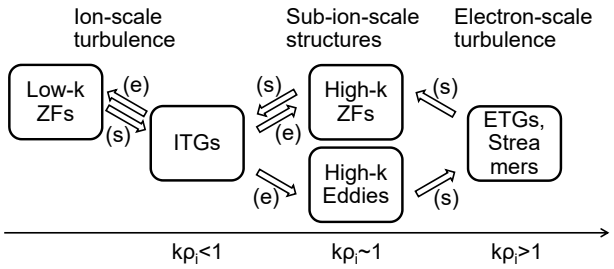

Figure 10. Schematic picture of the cross-scale interactions between ion-scale and electron-scale turbulence through sub-ion-scale structures. The symbols '(e)' and '(s)' denote the 'excitation' and 'suppressing' effects, respectively.

turbulence. Second, kinetic electrons in the ITG turbulence produce short-wave-length zonal flows (High-k ZFs), which tend to suppress ITGs and can be disturbed by the electron-scale turbulence. Through these processes, the electron-scale and ion-scale turbulence can interact. We emphasize the importance of sub-ion-scale structures around $k\rho_{\rm i} \simeq 1$ in cross-scale interactions, rather than long-range interactions in wave-number space.

We have newly developed the fluid approximation of triad transfer analysis and the sub-space transfer analysis techniques, to evaluate nonlinear cross-scale interactions in multi-scale turbulence. The fluid approximation significantly reduces computational cost and allows the analysis of triad transfer by post-processing, but is applicable only for qualitative analysis. Since the formulation is based on particle position fluid moments (not on gyrocenter fluid moments which cannot be measured in experiments), the fluid approximation of triad transfer can be experimentally evaluated, if fluid moments are measured with sufficient two-dimensional resolutions. The sub-space transfer, which does not necessarily require the fluid approximation, allows flexible analyses of interactions among arbitrary sub-spaces, and identifies collective behaviors of cross-scale interactions. Additionally, we here propose another class of sub-space transfer, which may be a convenient diagnostic tool of cross-scale interactions in gyrokinetic simulations with moderate computational costs. Dividing the wave-number space into two sub-spaces of ion and electron scales for evaluating $\mathcal{N}_{{\rm s}\boldsymbol{k}}^{\Omega_p,\Omega_q}$ of Eq. (34) by using FFT, one may obtain the following form of the entropy transfer,

$$J_{{\rm s}\boldsymbol{k}}^{\Omega_p,\Omega_q} = {\rm Re}\left[\left\langle \int dv^3 \frac{T_{\rm s}\tilde{g}_{{\rm s}\boldsymbol{k}}}{F_{\rm Ms}} \mathcal{N}_{{\rm s}\boldsymbol{k}}^{\Omega_p,\Omega_q} \right\rangle\right]. \tag{37}$$

It keeps only the symmetric property $J_{{\rm s}\boldsymbol{k}}^{\Omega_p,\Omega_q} = J_{{\rm s}\boldsymbol{k}}^{\Omega_q,\Omega_p}$ but not the detailed balance. The transfer $J_{\boldsymbol{k}}^{\Omega_i,\Omega_i}$ represents the net entropy gain/loss of the mode $\boldsymbol{k}$ from ion-scale turbulence, and $2J_{\boldsymbol{k}}^{\Omega_e,\Omega_i} + J_{\boldsymbol{k}}^{\Omega_e,\Omega_e}$ means the contributions in the presence of electron-scale turbulence.

The multi-scale turbulence paradigm is not limited to the case between ITG and ETG turbulence. For example, micro-tearing modes are characterized by an ion-scale poloidal wave number and a radially localized current sheet, which may be regarded as a sub-ion-scale structure and can be affected by the ETG turbulence. Not only micro-instabilities of electron and ion scales, interactions between ion-scale turbulence and global magneto-hydrodynamic instabilities are an alternative topic of interests [26].

Extensions of multi-scale plasma turbulence to other instabilities are remained for future works, and should provide more comprehensive understandings on cross-scale interactions.

Acknowledgments

This work was partially supported by MEXT FLAGSHIP 2020 project as a priority issue on the Post-K computer (Category 6-D), the MEXT KAKENHI Grant No. 26800283, and "Joint Usage/Research Center for Interdisciplinary Large-scale Information Infrastructures" and "High Performance Computing Infrastructure" in Japan. Computations were performed on the K computer at RIKEN Advanced Institute for Computational Science through the HPCI System Research Project (Project ID:hp120011,hp160208), the Helios at Computational Simulation Center of International Fusion Energy Research Centre (IFERC-CSC), and the Plasma simulator at National Institute for Fusion Science.

References

[1] Itoh S.-I., and Itoh K., 2001 *Plasma Phys. Control. Fusion* **43** 1055
[2] Li J. Q., and Kishimoto Y., 2002 *Phys. Rev. Lett.* **89** 115002
[3] Holland C., and Diamond P. H., 2004 *Phys. Plasmas* **11** 1043
[4] Jenko F., 2004 *J. Plasma Fusion Res. SERIES* **6** 11
[5] Candy J., Waltz R. E., Fahey M. R. and Holland C. 2007 *Plasma Phys. Control. Fusion* **49** 1209
[6] Waltz R. E., Candy J. and Fahey M. R. 2007 *Phys. Plasmas* **14** 056116
[7] Görler T. and F. Jenko 2008 *Phys. Rev. Lett.* **100** 185002
[8] Howard N. T., Holland C., White A. E., Greenwald M., and Candy J., 2014 *Phys. Plasmas* **21** 112510
[9] Howard N. T., Holland C., White A. E., Greenwald M., and Candy J., 2016 *Nucl. Fusion* **56** 014004
[10] Maeyama S., Idomura Y., Nakata M., Yagi M., and Miyato N., 2014 *Proc. 25th IAEA Fusion Energy Conf.* TH/1-1
[11] Maeyama S., Idomura Y., Watanabe T.-H., Nakata M., Yagi M., Miyato N., Ishizawa A., and Nunami M., 2015 *Phys. Rev. Lett* **114** 255002
[12] Holland C., Howard N. T., and Grierson B. A., 2016 *Proc. 26th IAEA Fusion Energy Conf.* TH/6-1
[13] Lenard A., and Bernstein I. B., 1958 *Phys. Rev.* **112** 1456
[14] Watanabe T.-H., and Sugama H., 2006 *Nucl. Fusion* **46** 24
[15] Maeyama S., Watanabe T.-H., Idomura Y., Nakata M., Nunami M., and Ishizawa A., 2015 *Parallel Comput.* **49** 1
[16] Sugama H., Watanabe T.-H., and Nunami M., 2009 *Phys. Plasmas* **16** 112502
[17] Maeyama S., Ishizawa A., Watanabe T.-H., Nakata M., Miyato N., Yagi M., and Idomura Y., 2014 *Phys. Plasmas* **21** 052301
[18] Tatsuno T., Barnes M., Cowley S. C., Dorland W., Howes G. G., Numata R., Plunk G. G., and Schekochihin A. A., 2010 *J. Plasma Fusion Res. SERIES* **9** 509
[19] Navarro A. Bañón, Morel P., Albrecht-Marc M., Carati D., Merz F., Görler T., and Jenko F., 2011 *Phys. Rev. Lett.* **106** 055001
[20] Nakata M., Watanabe T.-H., and Sugama H., 2012 *Phys. Plasmas* **19** 022303
[21] Hatch D. R., Jenko F., Navarro A. Bañón, and Bratanov V., 2013 *Phys. Rev. Lett* **111** 175001
[22] Scott B., 2010 *Phys. Plasmas* **17** 102306
[23] Cowley S. C., Kulsrud R. M., and Sudan R., 1991 *Phys. Fluids B* **3** 2767
[24] Dominski J., Brunner S., Görler T., Jenko F., Told D., and Villard L., 2015 *Phys. Plasmas* **22** 062303
[25] Jenko F., Dorland W., Kotschenreuther M., and Rogers B. N., 2000 *Phys. Plasmas* **7** 1904
[26] Ishizawa A., and Nakajima N., 2007 *Nucl. Fusion* **47** 1540